Characterization of Goldstrike ore carbonaceous material

Part 2: Physical characteristics

J.F. Stenebråten, W.P. Johnson and J. McMullen

Abstract

Carbonaceous material (CM) from the Barrick Goldstrike Mines, NV, was characterized with respect to its gold sorption (preg-robbing) and gold recovery behavior. The breadth of graphite peaks measured by X-ray diffraction were used to calculate crystallite dimensions (002) of the CM. The (002) dimension was found to vary inversely with preg-robbing activity and directly with gold-recovery behavior, indicating that the degree of graphitization (maturation) experienced by the carbonaceous material is correlated with gold-loss during ore processing. The inverse correlation of preg-robbing activity was improved when percent preg-robbing was regressed against (002) crystallite size and carbon content. The (101) crystallite dimensions of all samples were calculated from laser Raman analysis, and were not found to correlate with preg-robbing behavior of the CM. BET surface area and micropore size distribution results were affected by grinding history, negating comparison of these characteristics between samples.

Key words: Ore characterization, Gold ores, Carbonaceous ore, Preg-robbing

Introduction

Naturally occurring organic carbon is found in many sediment-hosted disseminated gold deposits (SHDG) within the Carlin trend in northeastern Nevada. It is on the Carlin trend that Barrick Goldstrike Mines Inc. (BGMI) resides. The natural organic carbon in these ores is strongly implicated in sequestration of gold during cyanide leaching, a phenomenon known as "preg-robbing" (Smith, 1968; Hausen and Bucknam, 1985). The organic carbon contents of the ores at BGMI range from about 8.3% to none detected. This results in a range of preg-robbing activities from high to low. High to low preg-robbing activities correspond to gold recoveries ranging from as low as ~20% to greater than 90%, respectively. The gold in the ore occurs as submicron elemental particles, and the majority is observed to be associated with sulfides, with most encapsulated in rims of arsenian framboidal pyrite (Wells and Mullens, 1973; Hausen and Park, 1985; Bakken et al., 1989; Chryssoulis et al., 1996). The encapsulation of the majority of gold within the sulfides requires oxidation of the gold-bearing sulfides to make the gold amenable for cyanide leaching. Hence, BGMI ores can suffer from two forms of refractoriness, originating from sulfide encapsulation of gold and from preg-robbing by carbonaceous matter in the ore. Sulfide refractoriness affects nearly all BGMI ores. Hence, autoclaving is used to release gold from sulfides. However, autoclaving does not appear to alleviate the preg-robbing that affects a significant portion of BGMI ores.

Many investigations have examined the structure and chemistry of carbonaceous matter in Carlin preg-robbing ores (Hausen and Bucknam, 1985; Hausen and Park, 1985). Some of these investigations have attributed the preg-robbing activity to humic acids in the carbon (Radtke and Scheiner, 1970). Subsequent studies have indicated that moieties previously thought to represent humic substances are from blast residues, such as ammonium nitrate and diesel fuel (Leventhal and Hofstra, 1990). Early studies indicated the presence of hydrocarbons within the organic carbon of Carlin ores (Radtke and Scheiner, 1970). Subsequent studies of other Carlin ores indicated a lack of hydrocarbons and have assigned a coal rank to the carbon ranging from semianthracite to anthracite (Hausen and Park, 1985) or from anthracite to graphite (Leventhal and Hofstra, 1990; Sibrell et al., 1990). The similarity between Carlin trend carbonaceous matter and activated carbon has also been noted (Nelson et al., 1986; Sibrell et al., 1990).

A trend in carbonaceous matter maturity exists from amorphous activated carbon to crystalline graphite, which is marked by increasing size of the crystallite of the carbon matrix. The unit structure formed as the carbon crystallizes is called a crystallite. As the organic material matures, the functional group content is reduced, and the crystalline structure becomes more ordered (Mantell, 1968). The final product of the maturation process is graphite with hexagonal unit cell structure and interlayer spacing (d-spacing) of 3.349 Å (Mantell, 1968). In a crystallite, many sheets comprised of hexagonal rings may be stacked in the dimension perpendicular to the hexagonal rings (L_c), and, likewise, many hexagonal rings may extend in the dimension parallel to the plane (L_a) of the hexagonal rings (Fig. 1). Both dimensions are known to increase with maturation (Mantell, 1968).

J.F. Stenebråten and **W.P. Johnson** are graduate student and assistant professor, respectively, with the Department of Geology and Geophysics, University of Utah, Salt Lake City, UT; **J. McMullen** , member SME, is senior manager of metallurgy with Barrick Gold Corp., Toronto, Canada. Nonmeeting paper number 98-319. Original manuscript submitted for review March 1998. Revised paper accepted for publication January 1999. Discussion of this peer-reviewed and approved paper is invited and must be submitted to SME prior to Aug. 31, 2000.

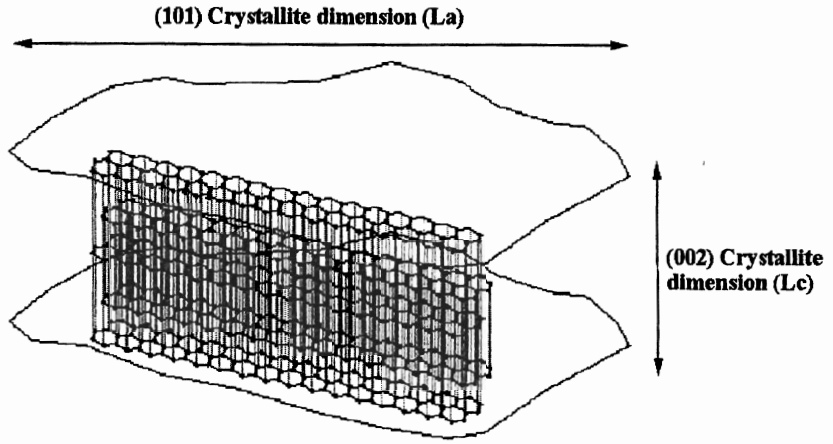

Figure 1 — Structural diagram showing crystallite dimension with graphite structure consisting of stacked sheets of aromatic rings.

Crystallite sizes for both the L_a and L_c dimensions can be calculated from peak shapes from X-ray diffraction (XRD), and the L_a dimension can also be measured by laser Raman spectroscopy. An inverse correlation between gold adsorption and crystallite size as determined by X-ray diffraction has been observed for commercial activated carbons (Miller and Sibrell, 1991).

The objective of this study is, therefore, to determine whether differences in the preg-robbing activity of Goldstrike ore correlate to the crystallite size of the carbon matrix. Miller and Sibrell (1991) performed gold adsorption studies on commercial carbons and correlated equilibrium sorption coefficients to various physical parameters of the carbon, including crystallite size, surface area, porosity and functional group content. The purpose of this study is to relate the same measured physical parameters to the preg-robbing and gold recovery behavior of Carlin carbonaceous ores. These correlations might then be used to aid in ore management. This strategy proceeds under the assumption that carbon is responsible for the observed preg-robbing and gold recovery behavior by virtue of its gold-uptake ability. Whereas Miller and Sibrell (1991) correlated physical parameters to equilibrium constants for gold adsorption to commercial carbon, this study seeks to correlate the behavior of the whole ore during processing to the physical characteristics of the carbon in the ore.

Methods

The present study was initiated to characterize the carbonaceous material in BGMI ores with respect to physical characteristics such as crystallite size, surface area and microporosity. This was done for the purpose of correlating physical characteristics of the carbonaceous matter to the preg-robbing behavior of the ore and to provide a basis for evaluating potential mechanisms of gold loss to the carbon. Chemical characteristics of the carbonaceous matter were measured and described in the first paper in this series (Stenebråten et al., 1999). In both studies, sixteen samples from the Betze-Post Mine and nearby exploration properties were studied. All samples were ground at BGMI prior to all analyses. Grinding was performed using TM pulverizers in the laboratory under dry conditions until 80% to 90% of the sample passed –200 mesh for all samples, except for those that were recovered from the mill grinding circuit as cyclone overflow (Samples #8 and #9). These latter samples yielded 80% (Sample #8) and 60% to 65% (Sample #9) passing –200 mesh. An additional coarse sample (Sample #11), dry ground to 100% passing -10 mesh, was used to examine the effect of grinding on the measured physical parameters

Preg-robbing behavior tests. Preg-robbing tests (Hausen and Bucknam, 1985), were performed on the ore samples by BGMI personnel prior to characterization by additional means described in this paper. There are two methods to evaluate preg-robbing behavior. The so-called preg-robbing test is quick and simple, and it evaluates preg-robbing in terms of percent gold-cyanide complex lost to the ore during batch equilibration. The second and more time-consuming test utilizes bench-top autoclaving followed by carbon-in-leach recovery (BTAC-CIL) of ore samples. This test evaluates preg-robbing behavior in terms of percent recovery of gold.

It is useful to distinguish between the two tests used to quantify preg-robbing behavior because the measured physical parameters correlate differently with the two tests. In the preg-robbing test, the head sample (5 g) is mixed with a gold-cyanide solution (10 mL at 3.0 ppm Au and 3,000 ppm NaCN), and equilibrated for 15 min. The solids are centrifuged down and gold is solvent-extracted from the supernatant and analyzed by AA spectrophotometry. The percent preg-robbing is determined by the difference between gold content of the spiked solution and the supernatant. In the recovery test, pulverized ore (200 g, 90% -150 mesh) is added to water (200 g), and sufficient sulfuric acid is added to dissolve carbonates. The slurry is blended (~15 min or until the pH is maintained between 1.5 and 2.0) and then diluted with water to ~500 g total weight. The temperature is maintained at 240°C with oxygen overpressure maintained at 4.206 MPa (610 psi) gage pressure for one hour. The slurry is then subjected to carbon-in-leach (CIL) by adding sodium cyanide (2.3 kg/t of slurry) and commercial activated carbon (12 g/L of slurry) and equilibrated for 16 hours while rolling. The carbon and slurry are filtered and gold is solvent-extracted from the supernatant and analyzed by atomic absorption (AA) spectrophotometry, whereas the gold content of the tails (filtered ore) and carbon are monitored by fire assay. Recovery is determined by the difference in gold content measured by fire assay between the initial head sample and the tails.

It is obvious that the BTAC-CIL recovery and percent preg-robbing tests differ in many important respects. The recovery test oxidizes sulfides to release gold, which is then solubilized in cyanide, whereas the percent preg-robbing test measures gold-cyanide complex $Au(CN)^-_2$ loss from a spiked solution. The mechanisms responsible for gold loss in these two tests are not necessarily the same. It is clear that the actual form of gold lost during the percent preg-robbing test is the gold-cyanide complex $Au(CN)^-_2$, whereas the form lost in the recovery test is unknown and may not be restricted to sorption of gold-cyanide complex to the carbon. However, it seems reasonable to expect that gold-cyanide, $Au(CN)^-_2$, is the operative gold complex in recovery tests. This presumption can be made on the basis that the equilibrium constant of $Au(CN)^-_2$ is ten orders of magnitude or more than other complexes hypothesized to occur as a result of autoclaving, i.e., thiosulfate or chloride complexes, (Nicol et al., 1987). For an extensive literature review of potential mechanisms of gold sorption to activated carbon, see McDougall and Hancock

Table 1 — Preg-robbing, recovery and Leco analysis before and after demineralization and density separation. Percent total carbon includes organic carbon and carbonates, and total sulfur includes both sulfates and sulfides. All analyses were performed by Barrick Goldstrike Metallurgical Services.

	Before demineralization						After demineralization		After demineralization and float-sink procedure			
Sample I.D.	Preg-robbing, %	Recovery, %	Total carbon, %	Organic carbon, %	Total sulfur, %	Sulfide sulfur, %	Total carbon, %	Organic carbon, %	Total carbon, %	Organic carbon, %	Total sulfur, %	Sulfide sulfur, %
#1	94.1	78.5	2.80	1.10	1.86	1.27	30.44	30.14	44.02	44.02	22.11	21.86
#2	9.16	73.4	1.00	1.00	2.78	2.65	14.78	14.78	26.05	26.05	26.24	25.61
#3	98.0	38.8	4.60	3.70	1.97	1.37	41.10	41.10	52.52	52.52	19.70	19.35
#4	61.8	61.8	2.10	0.60	1.71	1.24	11.72	11.68	20.98	20.98	28.80	27.61
#5	55.1	60.4	1.60	1.20	1.94	1.59	21.96	21.96	36.41	36.41	23.49	23.16
#6	98.0	40.3	5.20	0.40	1.97	1.54	17.62	17.62	30.48	30.48	23.57	23.03
#7	89.2	49.8	3.10	2.10	2.32	1.75	32.53	32.53	40.97	40.97	21.64	21.46
HPR-1	94.0	N/K	5.90	4.40	2.12	1.63	N/K	N/K	83.60	83.60	3.13	1.13
0421	95.2	N/K	7.92	7.92	1.46	0.63	N/K	N/K	67.11	67.11	12.38	N/K
0418	97.0	N/K	8.31	8.31	0.38	0	N/K	N/K	68.96	68.96	11.53	N/K
0415	98.0	N/K	9.07	3.02	0.40	0	N/K	N/K	68.33	68.33	10.25	N/K
#11	63.9	N/K	4.90	1.00	2.05	1.69	N/K	N/K	53.78	53.78	16.68	16.25
LPR-1	2.00	N/K	3.80	3.20	4.33	3.68	N/K	N/K	64.64	64.64	5.09	5.045
#8	5.00	91.6	N/K	0.30	N/A	2.75	2.50	2.46	11.34	11.34	28.21	26.21
# 9	5.00	92.8	N/A	0.20	N/A	2.40	4.85	4.85	13.32	13.32	31.02	30.17
0595	3.80	N/K	N/A	N/A	N/A	N/A	N/K	N/K	53.94	53.94	3.16	N/K

(1980), Adams and Fleming (1989), and Sibrell and Miller (1992). Both types of tests (preg-robbing and gold recovery) were performed by Barrick Metallurgical Services. Gold and carbon content of the ore was determined by fire assay and Leco analyses at BGMI.

Demineralization and density separation. It was necessary to remove silicates and carbonates originally in the Goldstrike ore, not only because of their interference with the XRD analysis for graphite, but also to enhance the resolution of other analyses of the carbonaceous material. Silicates and carbonates were removed by acid digestion, using hydrochloric acid (HCl), hydrofluoric acid (HF) and boric acid, according to the procedure of Tafuri (1987) and as described in detail in the first paper in this series (Stenebråten et al., 1999).

Following the acid digestion-demineralization procedure, the weight percent of organic carbon in the concentrate ranged from 2.46% to 41.10% (Table 1). The low preg-robbing samples, Samples #8 and #9, contained the least amount of carbonaceous material with sulfides being the major non-carbonaceous contributor to those concentrates. The low percentage of carbonaceous material resulted in a low signal during XRD analysis; hence, an increase of carbonaceous material concentration was desirable. Density separation by sodium polytungstate (SPT) ($3Na_2WO_4 9WO_3 H_2O$), by Sometu-US, resulted in sufficient separation for the purposes of this study, and this process is described in detail in the first paper of this series (Stenebråten et al., 1999). After density separation, the carbon content ranged from 11.34% to 83.60% (Table 1). This material, referred to as carbonaceous matter (CM), contains various sulfides such as pyrite, arsenopyrite and realgar (Stenebråten et al., 1999) in addition to carbon.

X-ray diffraction. XRD analyses were performed with a Rigaku DMAX 2200V diffractometer, using a copper anode. The diffractometer was operated at 40 kV and 30 mA with a start angle (2θ) of 15° and a stop angle of 80° (2θ). The step size was set at 0.01 with a scan speed of 5 deg/min and step time of 0.6 sec. The slit settings were as follows: divergence slit width at 1.0°, scatter slit width at 1.0° and receiving slit width at 0.15°.

The samples were mounted in a side-loaded sample holder after repeated sequential filling and tapping until the holder was filled. The above process was used to pack all samples to ensure similar surface textures and packing. Peak identification software (Jade+, Materials Data Inc.) was used to identify peaks, establish the baseline and measure the d-spacing and the full-peak-width at half-maximum-peak-height (FWHM).

The FWHM is characteristic of the average crystallite size, with a tall and narrow peak representing a larger crystallite size, while a broader peak of less intensity would be characteristic of a smaller crystallite. Each peak in the diffractogram represents refractions of distinct sets of planes. The (002) refraction represents the L_c dimension, while the (101) refraction represents the average dimension parallel to the plane of the hexagonal rings (L_a). From the FWHM, the average crystallite sizes can be calculated using the Scherrer equation (Warren, 1969), assuming that the crystallites are approximately cylindrical in shape

$$L_c(\text{Å}) = \frac{K\lambda}{\beta\cos\theta} \qquad (1)$$

where

K is equal to 0.89 for L_c,

θ is the incident angle corresponding to peak maximum intensity,

λ is the incident X-ray wavelength (1.540510 Å for copper source) and

β is the peak width at FWHM (radians).

Corrections for instrument broadening were performed by analyzing a lanthanum hexaboride standard and applying

$$\beta_c^2 = \beta_{peak}^2 - \beta_{standard}^2 \quad (2)$$

where

β_{peak} represents the peak width as observed in the diffractogram,

$\beta_{standard}$ is the peak width from the standard and

β_c is the corrected peak width used in Eq. (1).

The (101) refraction was not detected in any samples; hence, estimates of crystallite size by XRD were restricted to the (002) dimension.

The d-spacing, measured between atomic planes, was also calculated from the X-ray diffractogram by Bragg's Law

$$d = \frac{n\lambda}{2\sin\theta} \quad (3)$$

where

d is measured in Ångströms,

n is the order of the reflection,

λ is the incident X-ray wavelength and

θ is the peak location at maximum peak intensity.

Laser Raman. Raman spectroscopy has been widely used in coal and carbonaceous material characterization to examine crystallite size parallel to the plane of the hexagonal sheets (L_a) (Tuinstra and Koenig, 1970; Zerda et al., 1981; Leventhal and Hofstra, 1990). In contrast to infrared (IR), the symmetric aromatic-ring stretching peak at ~1,600 cm^{-1} is Raman active due to the variable polarizability of the C=C bond during stretching, and this peak dominates in highly ordered (highly crystalline) structures (Skoog and West, 1980). In less crystalline structures, a peak at 1360 cm^{-1} becomes prominent at the expense of the 1582 cm^{-1} peak (Tuinstra and Koenig, 1970). The ratio of the maximum Raman intensity at 1360 cm^{-1} to the maximum intensity at 1582 cm^{-1} has been used to determine the crystallite dimension (L_a) parallel to the plane of the aromatic sheets (101 dimension) (Tuinstra and Koenig, 1970). The empirical mathematical relationship between the 1,360 cm^{-1}/1,582 cm^{-1} peak ratio and the (101) crystallite dimension was found to be

$$L_a(\text{Å}) = 46\frac{I_{1582}}{I_{1360}} \quad (4)$$

where

I_{1582} and I_{1360} are the maximum peak intensity of the respective peaks and

L_a measured in Ångströms (Tuinstra and Koenig, 1970).

Lespade et al. (1982) modeled the theoretical relation between the 1,582 and 1,360 cm^{-1} peak intensities, as related to variations in the (101) crystallite size, to predict the Raman spectra arising from increasing crystallite disorder. Nakamizo et al. (1978) also showed this relation by dry-grinding to introduce crystallite disorder into Ceylon natural graphite.

Raman spectroscopic analyses were run with undiluted samples, because the desired scattered radiation increases with sample mass irradiated. The glass sample holder was inclined at 68° to form a focused laser stripe analyzed with 90° collection optics and a CCD detector (EG&G PARC) using a single-stage F/4 monochrometer (Spex). Scatter from the 530.9-nm line of a krypton ion laser (Coherent Innova 90) was filtered with a 5-mm YG-550 optical glass filter (Schott Glass). Laser power was set at 60 mW. Three scans were performed on each sample to eliminate spikes in the spectra caused by cosmic radiation.

BET surface area. A direct correlation between BET surface area and gold adsorption has been observed in carbons of decreasing surface area, in order from commercial activated carbons, carbon black, graphite and diamond, corresponding to decreasing gold sorption (Miller and Sibrell, 1991). BET surface area analyses were performed in this study of natural ore carbons using a Quantachrome OS-10 multipoint BET surface area analyzer using N_2 gas. Each sample was aerated and dried at 50°C for 15 min. to remove water vapor to avoid inaccurate sample weights and surface area measurements. The adsorption-desorption cycle was run twice before measurements were taken. Three points of adsorption and desorption (N_2 volume) were measured for each sample at ratios of adsorbate pressure vs. adsorbate saturated equilibrium vapor pressure equal to 0.05, 0.15 and 0.25. For each measurement, only the desorption recording was used for greater accuracy.

Pore size distribution. Micropores (pores less than 20 Å) are thought to govern the activity of commercial activated carbon with respect to adsorbing the gold cyanide complex (McDougall and Hancock, 1980). Six samples were analyzed for pore size distribution by N_2 gas adsorption at higher pressures relative to those used for surface area determination. Outgassing was performed at 25° C for 16 hours. Microporosity analyses were performed on an AUTOSORB gas sorption analyzer (Quantachrome Corp.), with partial pressure of N_2:He from 0.0001 to 1.00.

Results

X-ray diffraction. XRD diffractograms of demineralized and concentrated samples showed significant differences between HPR and LPR samples, as shown by spectra representative of the two groups (Fig. 2). The low preg-robbing samples (LPR) tended to show sharp graphite peaks, whereas the high preg-robbing samples (HPR) showed broad low graphite peaks. Sharper peaks indicate larger crystallite dimension. The (002) crystallite dimension, or L_c (Eq. (1)), ranged from 30 ± 6 Å for less crystalline samples to 373 ± 9 Å for highly crystalline samples (Table 2). The L_c (002) crystallite dimension for the CM was found to be inversely correlated with percent preg-robbing (-0.76 correlation coefficient) and directly correlated to percent BTAC-CIL gold recovery (+0.78 correlation coefficient) (Fig. 3). These results indicate that higher crystalline maturity is associated with the low preg-robbing samples, as has been observed for the adsorption of gold-cyanide complex, $Au(CN)^-_2$, on commercial activated carbon of widely varying crystallite sizes (Miller and Sibrell, 1991), ranging from 9.5 Å (activated carbon) to 190 Å (graphite). It is noteworthy that there appears to be a large decrease in percent preg-robbing above a crystallite size of about 100 Å. However, the crystallite size of the CM is not the only parameter affecting preg-robbing behavior of the ore (described below).

Along with the (002) crystallite size, the d-spacing of the carbonaceous samples was determined and found to decrease with increasing (002) crystallite size (Fig. 4 and Table 2). The graphitization of amorphous carbonaceous material is marked by an increase of crystallite size in all dimensions and a concomitant decrease in d-spacing (Mantell, 1968). The d-spacing values, therefore, corroborate the observed trend of

increased thermal maturity being associated with low preg-robbing behavior. For comparison, the (002) crystallite dimension for commercial carbon blacks has been reported to range from 12 to 27 Å and the d-spacing to range from 3.48 to 3.60 Å (Kinoshita, 1988). These values are comparable to the d-spacing values of the high preg-robbing Goldstrike CM, which range from 3.40 to 3.53 Å (Table 2). Dividing the L_c dimension by the d-spacing indicates that the Goldstrike CM particles consist of crystallites with 8 to 112 parallel layers of hexagonal sheet structures with random orientation within the planar layers of the crystallites. Random orientation within the planes is indicated by nondetectable L_a (101) peaks using XRD.

Laser Raman. Two dominant peaks at approximately 1,600 and 1,360 cm^{-1} were visible in the Raman spectra of all samples (Fig. 5). These results corroborate previous findings for carbon from the Carlin Mine (Leventhal and Hofstra, 1990). The Raman spectra from the low preg-robbing (LPR) samples were generally of poorer resolution relative to the high preg-robbing (HPR) samples, presumably due to lower carbon concentrations in LPR samples relative to HPR samples. From the relationship of the intensity ratio of the 1,360 and 1,600 cm^{-1} Raman peaks (Tuinstra and Koenig, 1970), the L_a (101) crystallite dimension can be calculated according to Eq. 4 (Table 2). Crystallite dimensions, L_a (101), for all samples were found to range from 40±1 to 45±1 Å (Table 2), indicating no variations among the HPR and LPR samples in the L_a (101) dimension. Since the L_c (002) crystallite dimension determined by X-ray diffraction shows large variation among the samples, it can be concluded that crystallite growth occurred preferentially in the L_c (002) dimension.

If gold loss is governed by characteristics of the carbon, it seems reasonable that the carbon content of the ore before demineralization, as well as a given measured characteristic (e.g., crystallite size of the carbon), may both be required in the correlation of these characteristics with preg-robbing behavior. As will be shown below, the measured surface area of the CM is directly correlated to its carbon content; hence, it would be incorrect to include measured surface areas with carbon content in such a correlation. The same would presumably be true of parameters such as total pore volume. Parameters such as crystallite size, average micropore size and atomic oxygen-carbon ratio would arguably be independent of carbon content; and hence, can be correlated along with carbon content against preg-robbing be-

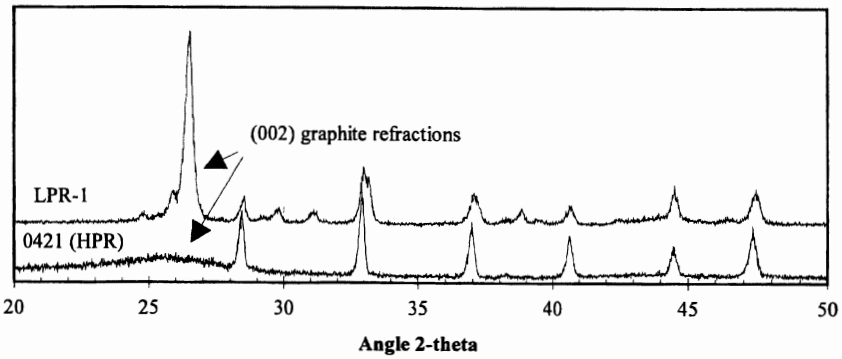

Figure 2 — XRD diffractogram of sample LPR-1 and 0421 (HPR) showing (002) graphite peak at 2q = 26.8°. Remaining peaks are due to sulfides still present in demineralized samples. The peak at 44.45° is due to refraction of aluminum sample holder and was used as internal standard (standard deviation of internal standard was found to be 0.000298 Å).

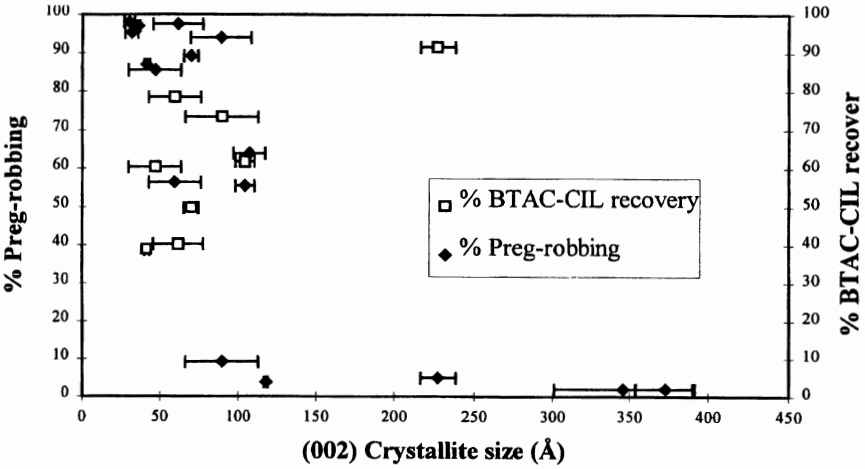

Figure 3 — Plot of (002) crystallite dimension vs. percent preg-robbing and percent BTAC-CIL recovery. Error bars denote standard deviation calculated from multiple analysis.

Table 2 — (002) crystallite dimension and d-spacing determined as by XRD analysis, and (101) crystallite dimensions as determined by laser Raman spectroscopy. Error estimates were based on standard deviations from multiple analysis.

Sample	(002) crystallite dimension, Å (L_c)	Cyrstallite d-spacing, Å (002)	(101) Crystallite dimension, L_a
#1	59.1 ± 16	3.47 ± 0.05	42.1 ± 0.6
#2	89.6 ± 23	3.43 ± 0.02	41.1 ± 0.1
#3	41.4 ± 2	3.53 ± 0.03	43.0 ± 0.9
#4	104.0 ± 6	3.45 ± 0.03	42.7 ± 0.6
#5	46.5 ± 16	3.50 ± 0.05	42.3 ± 0.4
#6	61.4 ± 16	3.49 ± 0.02	42.7 ± 0.7
#7	69.7 ± 4	3.46 ± 0.02	40.3 ± 0.6
HPR-1	88.8 ± 19	3.46 ± 0.01	44.9 ± 0.5
0421	31.7 ± 4	3.53 ± 0.02	43.7 ± 0.3
0418	35.7 ± 1	3.53 ± 0.01	42.4 ± 0.6
0415	30.3 ± 3	3.53 ± 0.02	42.4 ± 0.1
#11	106.9 ± 10	3.40 ± 0.01	42.3 ± 0.3
LPR-1	227.3 ± 11	3.35 ± 0.01	44.4 ± 0.6
#8	345.8 ± 45	3.34 ± 0.01	43.3 ± 1.4
#9	372.8 ± 19	3.36 ± 0.01	42.8 ± 0.3
0595	117.6 ± 1	3.42 ± 0.01	44.2 ± 0.4

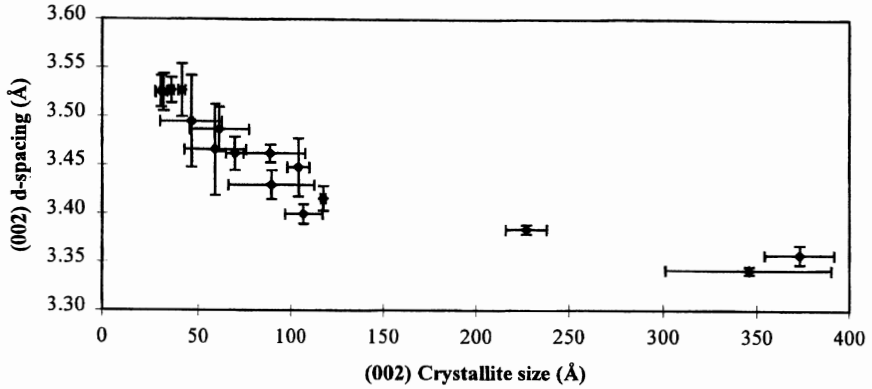

Figure 4 — Plot of (002) crystallite dimension vs. crystallite d-spacing. Error bars denote standard deviation calculated from multiple analysis.

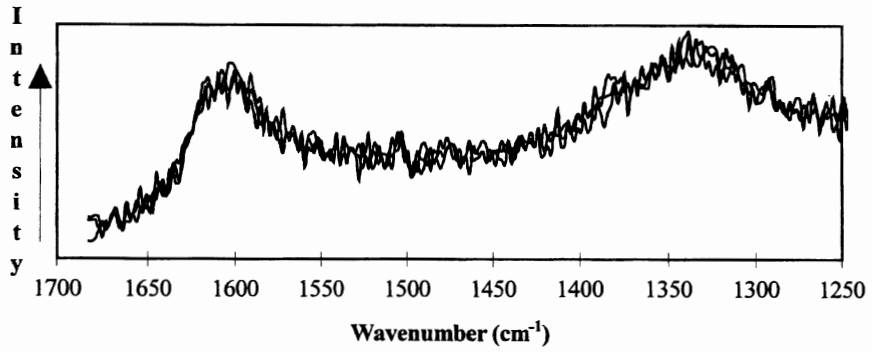

Figure 5 — Triplicates of Raman spectra of the sample 0421 (HPR), showing the two peaks characteristic for graphite at ~1600 cm^{-1} and 1360 cm^{-1}.

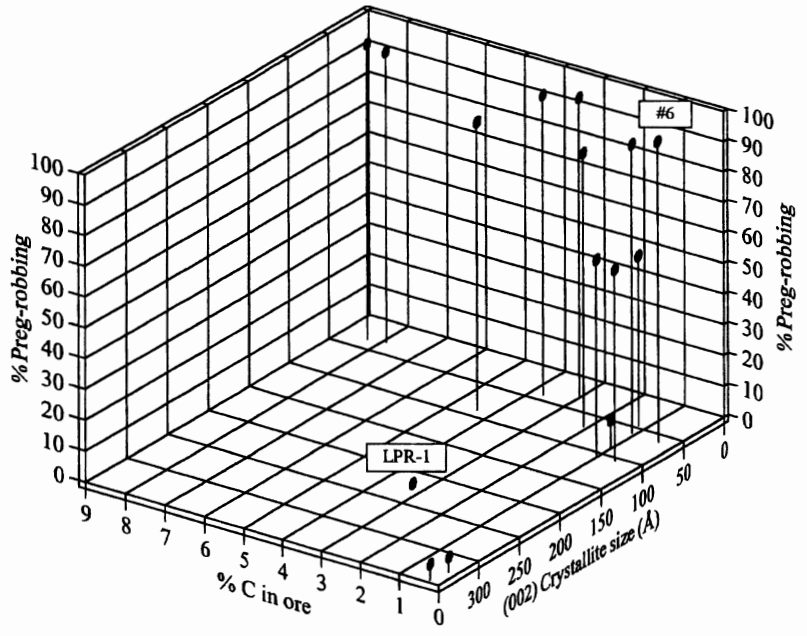

Figure 6 — Three-dimensional plot of percent preg-robbing vs. percent CM in ore and (002) crystallite size.

havior. The L_c (002) crystallite size is shown in the following section to be independent of grinding history in this study. As a result, this parameter is considered truly representative of the carbon.

Plotting both percent carbon (%C) of the non-demineralized ore and L_c (002) crystallite size vs. percent preg-robbing (Fig. 6) improves the correlation of preg-robbing behavior to L_c (002) crystallite size. As can be seen in Fig. 7, there is an apparent poor correlation of percent preg-robbing with ore carbon content (+0.50 correlation coefficient). However, there appears to be a nonlinear correlation, such that ores with more than 1% carbon tend to show high preg-robbing behavior. It is clear, however, that the combination of percent carbon and L_c (002) crystallite size best explains preg-robbing behavior. For example, Sample LPR-1 is not well explained by Fig. 7, because it shows an anomalously low preg-robbing behavior given its relatively high carbon content. However, Sample LPR-1 is well explained in Fig. 6 by virtue of the fact that it displays a large crystallite size. Likewise, Sample #6 shows anomalously high preg-robbing behavior relative to its low %C (Fig. 7) yet is well explained in Fig. 6 by its low L_c (002) crystallite size. Figure 6 indicates that ore with %C greater than ~1% and carbon crystallite size less than ~100 Å will display high preg-robbing behavior, whereas ores with %C less than ~1% and carbon crystallite size greater than ~200 Å will show low preg-robbing behavior. Statistical nonlinear correlation can be attempted when additional data have further constrained this response surface.

Plotting available results from BTAC-CIL recovery data against %C and L_c (002) crystallite size (Fig. 8) shows correlation of of BTAC-CIL recovery with %C and L_c (002) crystallite size (-0.62 and +0.78 correlation coefficients, respectively). The figure indicates that gold recovery decreases as %C increases and L_c (002) crystallite size decreases. Data values showing high percent preg-robbing also show a low percentage of BTAC-CIL recovery, corroborating the hypothesis that aurocyanide complex interaction with carbon is the dominant process of gold loss in the BTAC-CIL recovery test, as it is in the percent preg-robbing test. However, it is noteworthy that the BTAC-CIL recovery test shows apparent linear dependence on %C (Fig. 8), whereas the preg-robbing test correlates nonlinearly with %C (Fig. 6). Given the differences in the two methods of testing preg-robbing and recovery behavior, it may not be surprising that different dependencies on %C and L_c (002) are observed. The origin of these different degrees of dependence on %C between the two tests is unknown. However, it can be speculated that it is, at least, in part due to the autoclaving in the BTAC-CIL recovery test, which may alter the carbon, the gold complex formed or both. Subsequent studies will examine autoclaved carbons for the purpose of determining the effect of autoclaving on the carbon structure, chemistry and aurocyanide complex adsorption.

BET surface area. Surface areas of the demineralized samples ranged from 1.5 to 43.8 m^2/g (Table 3), increasing

with increasing carbon content, which indicates that better separation of sulfides from the organic carbon would be required to obtain a surface area truly representative of the carbon. Subsequent work will investigate methods of additional sulfide removal from these samples to determine surface areas representative of the carbon.

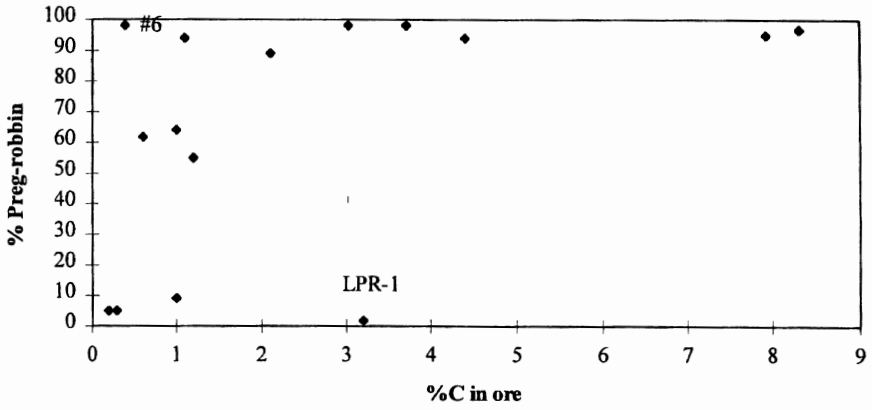

Figure 7 — Plot of percent carbonaceous matter in ore vs. percent preg-robbing. Error bars denote standard deviation calculated from multiple analysis.

Pore size distribution. Porosity analyses did not distinguish differences in pore types between HPR and LPR demineralized samples, as deduced from the hysteresis loop in N_2 adsorption-desorption (data not shown). HPR samples showed generally a lower total pore volume, ranging from 0.13 to 0.17 cm^3/g, relative to the lower preg-robbing samples, ranging from 0.25 to 0.31 cm^3/g (Table 4), except for Sample #9 (LPR), which had a total pore volume of 0.057 cm^3/g. However, the observed lower total pore volume in Sample #9 may be due to the lower percentage of carbonaceous material (Table 1), rather than to any differences in pore structure of the carbonaceous material. These values are small relative to commercial activated carbons, which may have total pore volumes ranging from 0.48 to 1.76 cm^3/g (Adams, 1989). The average pore diameter of the HPR demineralized samples was smaller, ranging from 257 Å to 313 Å, relative to the LPR demineralized samples, ranging from 519 to 566 Å (Table 4), indicating a possible inverse correlation between average pore size and preg-robbing behavior. However, the highest average pore diameter is associated with the MPR sample (1,050 Å), suggesting that additional samples are required to determine the existence of a trend. An inverse correlation between gold adsorption and micropore size was observed for commercial carbons ranging in average pore size from micropores (<20 Å diameter for activated carbons) to macroporous (>500 Å diameter for graphite) (Miller and Sibrell, 1991).

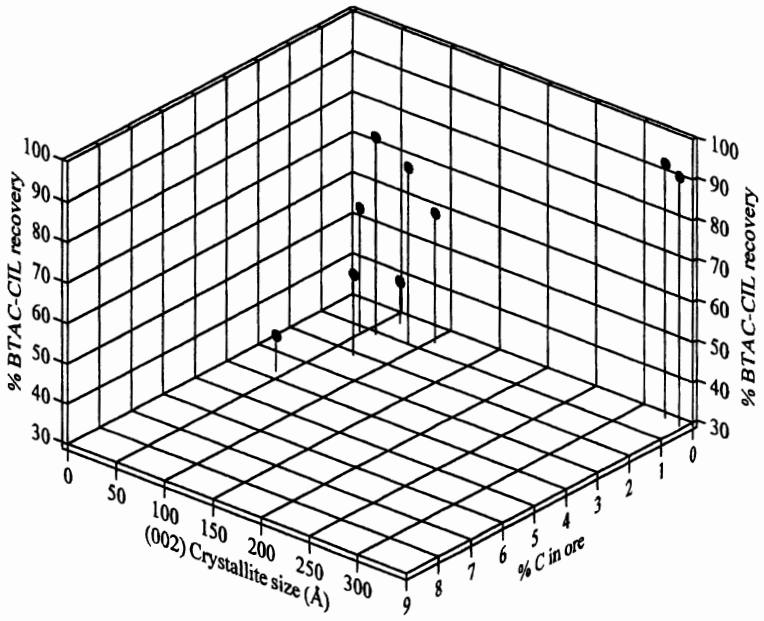

Figure 8 — Three-dimensional plot of percent BTAC-CIL recovery vs. percent CM in ore and (002) crystallite size.

Ball mill grinding experiment. Specific surface area and crystallite dimensions were shown to be altered by dry grinding of natural graphite using mortar and pestle (Nakamizo et al., 1978). Therefore, the effect of ore grinding was studied to determine the effect on the L_c, L_a, surface area and porosity of the demineralized samples. The demineralized, density-separated concentrate of Sample #11 was chosen for the experiment as it was the coarsest (-10-mesh) sample received from BGMI, and it would, therefore, best indicate any alteration by ball mill grinding. The mill (mild steel ball mill, 8 x 7 in., Sepor Inc.) was filled to approximately 10% media, by volume, with ceramic (0.5-in.-diam, bulk density = 2.0 g/cm^3) or steel balls (a mixture of diameters ranging from 0.5 to 1.5 in.), demineralized carbonaceous matter (100 g) and deionized water to form a paste. Mill speed was 70% of critical, and sampling of CM for determination of crystallite size was performed at 2, 4, 8, 16, 32, 64, 128, 256 and 512 min. XRD analysis did not show any change in the L_c (002) crystallite size as a result of the wet ball mill grinding by either ceramic or steel balls after (Table 5). The L_a (101) crystallite dimension measured by laser Raman spectroscopy was also unchanged by ball mill grinding (Table 5). Average pore size, total pore volume and BET surface area were strongly affected by grinding (Table 5). As a result, comparison of surface area and average pore sizes between samples with differing grinding histories appears invalid. The discrepancy between grinding effects on crystallite size observed in Nakamizo et al. (1978) vs. this study is unexplained. Because the samples were ground prior to preg-robbing tests, the observed relationships between L_c (002) crystallite size and percent preg-robbing (and BTAC-CIL recovery) are valid, regardless of whether grinding actually affects crystallite dimension.

Discussion

The correlation of L_c (002) crystallite size and %C to percent preg-robbing indicates that the preg-robbing mechanism may be related to aurocyanide-active structures in the carbon that decrease as the L_c (002) dimension increases. The potential mechanism of aurocyanide complex uptake by Goldstrike ore carbonaceous material can be discussed based on the uptake of gold-cyanide complex by commercial acti-

Table 3 — BET surface area results with carbon content shown for comparison.

Sample	BET surface area, m^2/g	Percent organic carbon in CM
#1	20.8	30.14
#2	8.3	14.78
#3	20.8	41.10
#4	7.3	11.68
#5	14.9	21.96
#6	12.7	17.62
#7	19.4	32.53
HPR-1	32.1	83.60
0421	42.9	67.11
0418	43.9	68.96
0415	41.2	68.33
# 11	13.4	53.78
LPR-1	34.7	64.64
#8	1.5	2.46
#9	1.6	4.82
0595	22.9	53.94

Table 4 — Micropore results prepared by Quantachrome Corp. Laboratories. Error estimates were based on standard deviations from multiple analysis.

Sample	Total pore Volume, cm^3/g	Average pore diameter, Å
#3	0.1708 ± 0.005	257 ± 8
#7	0.1369 ± 0.004	314 ± 9
#9	0.0566 ± 0.001	519 ± 16
#11	0.3127 ± 0.009	1,050 ± 32
LPR-2	0.2521 ± 0.007	566 ± 17

Table 5 — Crystallite size of (002) and (101) dimensions, BET surface area and micropore results of sample before and after ball mill experiment. Error estimates were based on standard deviations from multiple analysis.

Results	Sample #11	Sample #11 after ball mill grinding
L_c, Å	106.9 ± 10	108.7 ± 9
L_a, Å	42.3 ± 0.3	42.0 ± 1
BET surface area, m^2/g	11.9 ± 0.4	19.6 ± 0.6
Total pore volume, cm^3/g	0.313 ± 0.009	0.245 ± 0.007
Average pore diameter, Å	1,050 ± 32	499 ± 15

vated carbons and graphites because the Goldstrike carbon is chemically equivalent to high aurocyanide-affinity commercial activated carbons (Stenebråten et al., 1998). It was shown in batch studies with highly oriented pyrolitic graphite that the sorption of gold-cyanide complex to graphite occurs preferentially at the crystallite edges (Sibrell and Miller, 1992). Likewise, Hennig (1961) showed that the edge sites of a single graphite crystal were at least 20 times more reactive than the basal plane. Adams (1989) observed that for a series of commercial activated carbons, $Au(CN)^-_2$ uptake was correlated with total micropore volume, thus, giving rise to the most widely accepted proposed mechanism of gold adsorption by commercial activated carbon under plant conditions. This mechanism is the association of gold-cyanide ion pairs with carbon by way of solvation in micropores (Adams, 1989). The walls of the micropores display polarity originating from carbon-oxygen functionality in the form of quinone or lactone structures (Adams, 1989).

It is clear, then, that a prevalence of microporosity and edge sites are related to aurocyanide uptake by activated carbon. However, Goldstrike ore carbon shows negligible microporosity, and, furthermore, the different crystallite structures (Fig. 9) show no easily predictable differences in edge-site content. Dividing the L_c dimension by the d-spacing (Table 2) indicates that the high preg-robbing (HPR) crystallites consist of around eight parallel aromatic layers, whereas there are about 112 layers in low preg-robbing (LPR) crystallites, with equivalent diameters for the two types of crystallites being indicated by laser Raman spectroscopy. Because the less-active larger crystallites show thicker edges relative to more active smaller crystallites, the overall area represented by edge sites in the two types of samples is difficult to predict. It is speculated, however, that the high $Au(CN)^-_2$ uptake by the smaller crystallites derives from irregularities in the edges of those crystallites.

The larger d-spacing, due to weaker C-C bonding in the L_c (002) dimension of the smaller crystallites is hypothesized to allow the occurrence of defects and irregularities in the crystallite edge (Pierson, 1993), resulting in a "ragged" edge in the mesopores formed between the smaller crystallites. In contrast, the larger crystallites, which have a smaller d-spacing, are hypothesized to display a cleaner "sheer" edge that is less active in the uptake of gold-cyanide complex. The high aurocyanide uptake in the smaller crystallite edges might then be explained by increased wall potential on shelves exposed on the "ragged" edges.

This interaction might be less strong than solvation by micropores in commercial activated carbon, in agreement with studies showing commercial carbon to have an equilibrium aurocyanide uptake constant that was ten times greater than the uptake constant shown by Carlin carbonaceous ores (Hausen and Bucknam, 1985). Subsequent studies will examine the equilibria and kinetics of aurocyanide complex interaction with LPR and HPR CM and commercial activated carbon, and relate these behaviors to their physical characteristics.

Conclusions

Based on these analyses of the physical parameters, it is concluded that the preg-robbing characteristics of Goldstrike ore were inversely correlated to the L_c (002) crystallite dimension calculated from XRD analysis. No differences among the samples were detected in the L_a (101) crystallite dimensions calculated from laser Raman spectroscopic analyses. Because the L_c (002) crystallite dimension was observed to vary among the samples, it is concluded that crystallite growth occurred preferentially in the L_c (002) dimension.

Surface area and pore size analyses were affected by grinding history and could not be compared between samples. Percent carbon (%C) of the ore was inversely and nonlinearly correlated with percent preg-robbing, and the combination of

%C and L_c (002) crystallite size appear to best explain the preg-robbing behavior.

The L_c (002) crystallite size of the carbon was directly correlated to BTAC-CIL recovery. Percent carbon in the ore was inversely correlated with BTAC-CIL recovery, and this apparent linear relationship, in contrast to the strongly non-linear relationship between %C and percent preg-robbing, may indicate different mechanisms of gold interaction with carbon between the two types of preg-robbing tests.

Acknowledgements

The authors wish to acknowledge and thank Barrick Goldstrike Mines for funding this project, and the authors wish to acknowledge the staff at Barrick Goldstrike Metallurgical Services for collecting samples and providing metallurgical and LECO analysis. The authors would also like to thank the following individuals: Dr. William Parry, Department of Geology and Geophysics, University of Utah, for helpful advice throughout the study and for access to the X-ray diffractometer and atomic adsorption spectrophotometer; Dr. Saskia Duyvesteyn, Department of Metallurgical Engineering, University of Utah, for advise and corrections; Philip L. Sibrell for helpful advice through the course of the project; Dr. Jan Miller, Department of Metallurgical Engineering, University of Utah, for providing access to the BET surface area analyzer, and Lydia Olson, Department of Chemistry, University of Utah, for access to the Raman spectroscope.

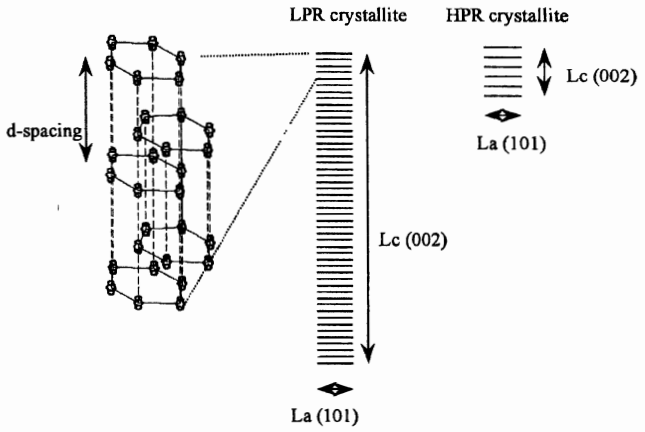

Figure 9— Figure showing stacking of hexagonal graphite rings, with d-spacing, and the relative size difference of LPR and HPR crystallites.

References

Adams, M.D., 1989, Ph.D. Dissertation, University of the Wiitwatersrand, Johannesburg, 387 pp.

Adams, M.D., and Fleming, C.A., 1989, "The mechanism of adsorption of aurocyanide onto activated carbon," *Metallurgical Transactions*, Vol. 20, B, pp. 315-325.

Bakken, B.M., Hochella, M.F., Jr., Marshall, A.F., and Turner, A.M., 1989, " High-resolution microscopy of gold in unoxidized ore from the Carlin Mine, Nevada," *Economic Geology*, Vol. 84, pp. 171-179.

Chryssoulis, S., Weisener, C., and Wong, C, 1996, "Deportment of gold in composites HPR-1 and LPR-1 of Goldstrike," Barrick Goldstrike unpublished company report, 10 pp.

Hausen, D.M., and Bucknam, C.H., 1985, "Study of preg-robbing in the cyanidation of carbonaceous gold ores from Carlin, Nevada," *Applied Mineralogy, Proceedings of the Second International Congress on Applied Mineralogy*, W.C. Park, D.M. Hausen, and R.D. Hagni, eds., AIME, Warrendale, PA, pp. 833-856.

Hausen, D.M., and Park, W.C., 1985, "Observations on the association of gold mineralization with organic matter in Carlin-type ores," *Organics and Ore Deposits*, W.E. Dean, ed., Denver Region Exploration Geologists Society, Wheat Ridge, CO, pp. 119-136.

Hennig, G.R., 1961, *Journal de Chimie Physique*, Vol. 58, No. 12, pp. 12-19.

Hennig, G.R., 1962, *Proceeding of the 5th Conference on Carbon*, Vol. 1, Pergammon Press, New York, p. 143.

Kinoshita, K., 1988, *Carbon — Electrochemical and Physicochemical Properties*, Wiley & Sons, New York, pp. 31-35.

Lespade, P., Al-Jishi, R., and Dresselhaus, M.S., 1982, "Model of Raman scattering from incompletely graphitized carbons," *Carbon*, Vol. 20, No. 5, pp. 427-431.

Leventhal, J., and Hofstra, A., 1990, "Characterization of carbon in sediment-hosted disseminated gold deposits, north-central Nevada," Gold '90, SME Symposium, Salt Lake City, UT, pp. 365 - 368.

Mantell, C.L., 1968, *Carbon and Graphite Handbook*, Interscience Publishers, New York, pp. 8 - 21.

McDougall, G.J., and Hancock, R.D., 1980, "Activated carbons and gold — a literature survey," *Mineral Science Engineering*, Vol. 12, No. 2, pp. 85-99.

Miller, J.D., and Sibrell, P.L., 1991, "The nature of gold adsorption from cyanide solutions by carbon," *EPD Congress '91*, The Minerals, Metals & Materials Society, Warrendale, PA, pp. 647-663.

Nakamizo, M., Honda, H., and Inagaki, M., 1978, "Raman spectra of ground natural graphite," *Carbon*, Vol. 16, pp. 281-283.

Nelson, J.H., MacDougall J.J., Baglin, F.G., Freeman D.W., Nadler, M., and Hendrix, J.L., 1982, "Characterization of Carlin-type gold ore by photoacoustic, Raman and EPS spectroscopy," *Applied Spectroscopy*, Vol. 36, pp. 574-576.

Nicol, M.J., Fleming, C.A., and Paul, R.L., 1987, "The chemistry of the extraction of gold," *The Extractive Metallurgy of Gold in South Africa. Johannesburg*, Vol. 1, G.G Stanley, ed., South African Institute of Mining and Metallurgy, pp. 831-905.

Pierson, H.O., 1993, *Handbook of Carbon, Graphite, Diamond and Fullerenes, Properties Processing and Applications*, Noyes Publications, Park Ridge, NJ, pp. 46-49.

Radtke, A.S., and Scheiner, B.J., 1970, "Studies of hydrothermal gold deposition (I). Carlin gold deposits, Nevada: The role of carbonaceous materials in gold deposition," *Economic Geology*, Vol. 65, pp. 87-102.

Sibrell, P.L., and Miller, J.D., 1992, "Significance of graphitic structural features in gold adsorption by carbon," *Minerals and Metallurgical Processing*, Vol. 9, No. 4, November, pp. 189-195.

Sibrell, P.L., Wan, R.Y., and Miller, J.D., 1990, "Spectroscopic analysis of passivation reactions for carbonaceous matter from Carlin trend ores," Gold '90, SME Symposium, Salt Lake City, UT, pp. 355 - 363.

Skoog, D.A, and West, D.M., 1980, *Principles of Instrumental Analysis*, 2nd ed., Saunders College, Philadelphia, pp. 265-270.

Smith, G.C., 1968, "Discussion of refractory ore," Carlin Gold Mining Company, Feb. 20, unpublished report.

Stenebråten, J.F., Johnson, W.P., and Brosnahan, D., 1998, "Characterization of Goldstrike ore carbonaceous matter, Part 1: Chemical characteristics," *Minerals & Metallurgical Processing*, Vol. 16, No. 3, August, pp. 37-43.

Tafuri, W.J., 1987, "Geology and geochemistry of the Mercur district, Utah," Ph.D. Dissertation, University of Utah, Salt Lake City, pp. 126-127.

Tuinstra, F., and Koenig, J.L., 1970, "Raman spectrum of graphite," *The Journal of Chemical Physics*, Vol. 53, No. 3, pp. 1126-1130.

Warren, B.E., 1969, *X-ray Diffraction*, Addison-Wesley, Reading, MA, pp. 251-262.

Wells, J.D., and Mullens, T.E, 1973, "Gold-bearing arsenian pyrite determined by microprobe analysis, Cortez and Carlin gold mines, Nevada," *Economic Geology*, Vol. 68, pp. 187-201.

Zerda, T.W., Andrzej, J., and Chmura, K., 1981, "Raman studies of coal," *Fuel*, Vol. 60, pp. 375-378.